Ordered and disordered phases in Al-Ni-Co decagonal quasicrystals

K. Edagawa, H. Tamaru, S. Yamaguchi, K. Suzuki, and S. Takeuchi
Institute for Solid State Physics, The University of Tokyo, Roppongi, Minato-ku, Tokyo 106, Japan
(Received 6 June 1994)

The composition ranges of Al-Ni-Co decagonal quasicrystals in superlattice-ordered and disordered states have been investigated. The single-decagonal-phase region is limited to a very small area around $Al_{71}Ni_{16}Co_{13}$ at 650 °C, which expands along an almost Al-constant line at 850 °C. The single-decagonal-phase area at 650 °C entirely yields the completely ordered state, while that at 850 °C yields either a partially ordered state or the completely disordered state. The real-space structural change between the ordered and disordered states has been investigated by high-resolution transmission electron microscopy (HRTEM). The HRTEM images for both states comprise the arrangements of ringlike contrasts, forming tiling patterns with the edge length of about 20 Å. These tiling patterns have been analyzed on the basis of a high-dimensional description of the quasicrystalline structure. The analysis has revealed that the two tiling structures have characteristic features of the ordered and disordered quasicrystalline lattices, respectively. This leads to the conclusion that the rearrangement of the atomic clusters giving the ring contrasts in the HRTEM image is responsible for the present order-disorder structural transformation, which is a new type of order-disorder transformation characteristic of quasicrystals.

I. INTRODUCTION

The decagonal phase is a two-dimensional quasicrystal, the structure of which has a periodicity along its tenfold axis and a quasiperiodicity in the plane perpendicular to it. The decagonal phase has first been discovered as a metastable phase in a rapidly solidified Al-Mn alloy.[1] Subsequently, thermodynamically stable decagonal phases have been found in Al-Cu-Co,[2] Al-Ni-Co,[2] Al-Cu-Rh,[3] Al-Ni-Rh,[3] and Al-Pd-M (M = Mn, Fe, Ru, and Os) alloys,[4,5] which have greatly advanced our understanding of the decagonal quasicrystalline structure.[6] Good-quality samples produced for these alloys have provided reliable structural information through single-crystal x-ray diffractometry and high-resolution transmission electron microscopy (HRTEM). On the basis of the structural information, a number of structure models have been proposed.[7] The decagonal phases found so far have various periodic lengths along the tenfold axis: about 4, 8, 12, and 16 Å. It is considered that all these phases have a stacking structure of planar atomic layers with a spacing of about 2 Å and that a variety of stacking sequences of different atomic layers result in the periods of even multiples of the spacing. HRTEM studies have shown that the structures of the decagonal phases can well be described as packing of columnar atomic clusters which themselves have fivefold or tenfold symmetry.[7-10]

In general, the structure of a quasicrystal can be described as a section of a high-dimensional periodic structure.[11,12] This fact allows us to extend the concept of superlattice order in ordinary crystals to quasicrystals. The superlattice order in a quasicrystal is defined as the superlattice order in the high-dimensional periodic lattice. In a previous paper, we have reported in an Al-Ni-Co alloy a new type of decagonal phase having such kind of superlattice order.[13] In subsequent studies, we have characterized the superlattice structure by electron- and x-ray-diffraction experiments[14] and investigated the temperature dependence of the degree of order[15] and the order-disorder transformation induced by electron-beam irradiation.[16] This type of superlattice order is essentially the same as that previously discussed by Ishihara and Yamamoto using two-dimensional generalized Penrose tilings.[17] Niizeki has studied theoretically this superlattice order in a more generalized fashion.[18] Detailed discussion on the diffraction pattern of the superlattice structure has recently been made by Lancon *et al.*[19]

The purpose of the present study is twofold: one is to investigate the formation ranges of the decagonal phases with and without the superlattice order in the Al-Ni-Co system and the other is to investigate the difference in the real-space structure between the ordered and disordered decagonal phases by HRTEM observation.

II. EXPERIMENTAL PROCEDURES

Al-Ni-Co ternary alloys with compositions ranging from 10 to 22 at. % Ni and from 8 to 20 at. % Co were prepared from the elemental constituents by arc melting under an argon atmosphere. Pieces cut from the alloy ingots were subjected to single-roller melt-spinning in an argon atmosphere, where the tangential speed of the copper roller was 39 m/s. The melt-spun samples were annealed at 650 °C for 72 h or at 850 °C for 4 h, after being sealed in an evacuated quartz ampoule, followed by water quenching.

Powder x-ray-diffraction experiments were carried out for the as-spun and annealed samples using Cu $K\alpha$ radiation to examine the phase constitution in the samples. To distinguish between the ordered and disordered decagonal phases, electron-diffraction experiments were performed using a JEOL 2000 FX transmission electron microscope (TEM) operating at 200 kV. High-resolution electron microscopic images were observed for the two

decagonal phases using a Hitachi H-9000 TEM operating at 300 kV. The samples for the TEM experiments were prepared by dispersing powdered materials on a microgrid mesh with collodion film.

III. RESULTS AND DISCUSSION

A. Al-Ni-Co Phase diagram around the decagonal phase region

Figures 1(a)–1(c) show examples of x-ray-diffraction spectra for the 650 °C-annealed samples. The labels D, O, H, and U denote decagonal phase, $Al_3(Ni,Co)$ phase isostructural with Al_3Ni orthorhombic phase,[20] $Al_3(Ni,Co)_2$ phase isostructural with Al_3Ni_2 hexagonal phase,[20] and an unidentified phase, respectively. For the unidentified phase, the peaks could not be indexed to any known binary Al-(Ni,Co) or ternary Al-Ni-Co phases.

Figures 2(a) and 2(b) show isothermal sections of the ternary phase diagram estimated from the results of the x-ray-diffraction measurements. Solid circles indicate the compositions examined. The phase boundaries are determined in view of the phase constitution, including the fraction of the phases, in each sample. The fraction of the phases was estimated from the intensity ratios in the diffraction peaks. We find that the single-decagonal-phase region is limited to a very small area around $Al_{71}Ni_{16}Co_{13}$ at 650 °C, but expands almost along an Al-constant line at 850 °C. It should be noted that the single-decagonal-phase area for the as-spun samples is very large; no trace of contaminant phases was detected for all the as-spun samples except $Al_{65}Ni_{35-x}Co_x$ ($x=15$ and 20), $Al_{67}Ni_{19}Co_{14}$, and $Al_{70}Ni_{10}Co_{20}$. The superlattice peaks of the ordered decagonal phase are so weak that the conventional powder x-ray-diffraction experiment cannot distinguish it from the disordered decagonal phase. To distinguish between them, electron-diffraction experiments were carried out for some of the samples.

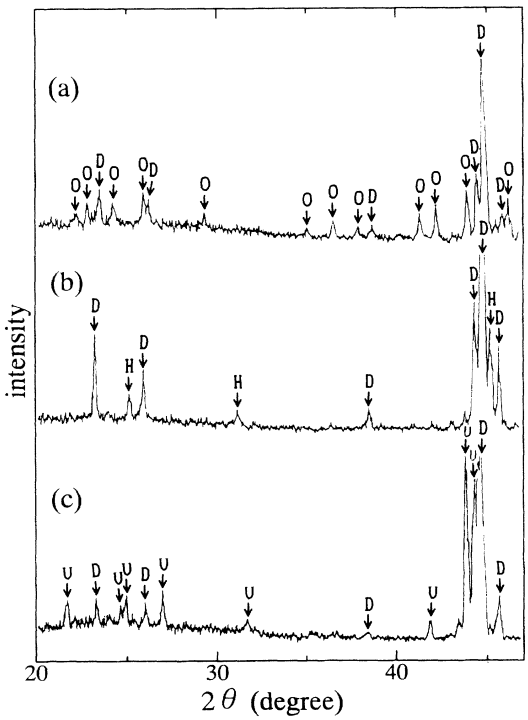

FIG. 1. X-ray-diffraction spectra measured for 650 °C-annealed samples with the compositions of $Al_{72}Ni_{16}Co_{12}$ (a), $Al_{70}Ni_{20}Co_{10}$ (b), and $Al_{70}Ni_{15}Co_{15}$ (c). The labels D, O, H, and U denote decagonal phase, orthorhombic $Al_3(Ni,Co)$ phase, hexagonal $Al_3(Ni,Co)_2$ phase, and an unidentified phase, respectively.

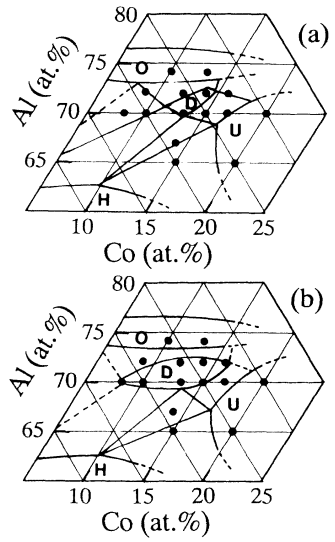

FIG. 2. Isothermal sections of the Al-Ni-Co phase diagram at 650°C (a) and at 850 °C (b). The labels D, O, H, and U denote decagonal phase, orthorhombic $Al_3(Ni,Co)$ phase, hexagonal $Al_3(Ni,Co)_2$ phase, and an unidentified phase, respectively. Solid circles indicate the compositions of the samples studied.

Figures 3(a)–(c) show typical examples of a tenth part of the tenfold electron-diffraction pattern of the decagonal phase. We see no noticeable difference in the arrangement of intense spots for these patterns. However, we can detect many additional weak spots in the patterns (a) and (b) which do not appear in the pattern (c). In addition, a remarkable difference is found in the arrangement of the weak spots between the patterns (a) and (b).

In previous papers,[14,15] we have given detailed discussion on the relation between the diffraction patterns of the ordered and disordered decagonal phases, which is briefly reviewed in the following. In general, the spot positions of the tenfold diffraction pattern of the decagonal phase are given by integer-coefficient linear combinations of four of the five center-to-vertex vectors of a regular pentagon. The spot intensity is strongly correlated with the phason momentum $G_\perp$[21]; spots with large $G_\perp$ are always weak. This fact allows us to assume some threshold value of $G_\perp$ in calculating the diffraction pattern; spots with larger $G_\perp$ than the threshold value can be omitted in the calculation. In Fig. 4, a calculated diffraction pattern is presented, in which $\mathbf{p}_i^{*\prime}$ ($i=1,\ldots,4$) in the figure are adopted as the basis vectors and a certain threshold value of $G_\perp$ is assumed. The reciprocal lattice spaned by $\mathbf{p}_i^{*\prime}$ includes the lattice spanned by $\mathbf{p}_i^*$ as a sublattice. More

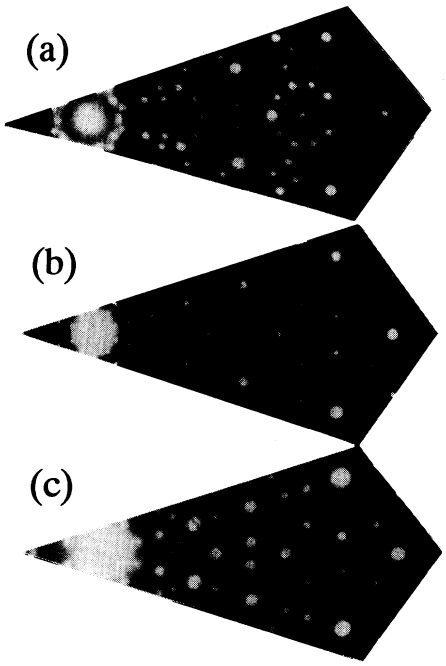

FIG. 3. $\frac{1}{10}$ sections of the tenfold electron-diffraction patterns for the 650 °C-annealed $Al_{70}Ni_{17}Co_{13}$ (a), 850 °C-annealed $Al_{70}Ni_{17}Co_{13}$, (b) and 850 °C-annealed $Al_{70}Ni_{22}Co_8$ (c) samples. The spot corresponding to the lattice spacing of about 2.0 Å is indicated by an arrowhead.

specifically, the reciprocal lattice spanned by $\mathbf{p}_i^{*\prime}$ can be classified into three groups, one of which coincides with the lattice spanned by $\mathbf{p}_i^*$. The classification is made in view of the sum of the indices referred to the basis vectors $\mathbf{p}_i^{*\prime}$: main spots satisfying $\sum_i h_i = 0$ (mod 5) (this group corresponds to the lattice spanned by $\mathbf{p}_i^*$) and two groups of superlattice spots satisfying $\sum_i h_i = \pm 1$ (mod 5) (hereafter denoted as S1) and ± 2 (mod 5) (S2), respectively. The reciprocal basis vectors of the ordered and disordered decagonal quasicrystalline structure correspond to $\mathbf{p}_i^{*\prime}$ and $\mathbf{p}_i^*$, respectively.

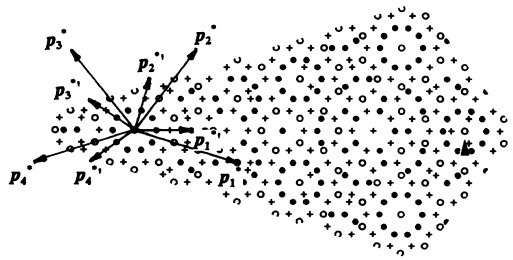

FIG. 4. A tenth section of a calculated tenfold diffraction pattern. $\mathbf{p}_i^{*\prime}$ and $\mathbf{p}_i^*$ span the reciprocal lattices for the ordered and disordered phases, respectively. By comparison with the observed patterns, $|\mathbf{p}_i^*|$ is evaluated to be about 1.0 $Å^{-1}$. The spot corresponding to the lattice spacing of about 2.0 Å is indicated by an arrowhead. Open circles, solid circles, and crosses represent main, S1, and S2 spots, respectively (see text).

Comparing the patterns in Figs. 3 (a)–(c) with the calculated pattern in Fig. 4, we find that the patterns (a), (b), and (c) consist, respectively, of all the three groups of spots, of only the main and S1 spots and of the main spots exclusively. The three structures correspond to the completely ordered state, a partially ordered state and the completely disordered state, respectively. Recently, we have studied by single-crystal x-ray diffractometry the temperature dependence of the degree of order for the superlattice-ordered decagonal phase of an $Al_{70}Ni_{17}Co_{13}$ alloy.[15] The experiment has shown that the two kinds of superlattice peaks, S1 and S2, behave differently against temperature; on raising the temperature S2 peaks start to lose intensity at a temperature between 700 and 750 °C and vanish almost completely at a temperature between 800 and 850 °C, while S1 peaks preserve about 40% of the original intensity even at 900 °C. The result that only S2 spots disappear in Fig. 3(b) is consistent with the temperature dependence of the two kinds of superlattice peaks shown in the x-ray-diffraction experiment.

Figure 5 shows the composition ranges of the three states estimated from the results of electron-diffracton experiments. Solid circles indicate the compositions of the samples for which the electron-diffraction experiment was carried out. For the compositions in two- or three-phase region in Fig. 5, we assumed that the composition of the decagonal phase in the sample is at the point on the phase boundary nearest to the sample composition. The single-decagonal-phase area at 650 °C entirely yields the completely ordered state, while that at 850 °C yields either the partially ordered state where S2 spots disappear or the completely disordered state where both S1 and S2 spots disappear. For the 850 °C-annealed $Al_{70}Ni_{20}Co_{10}$, which lies on the boundary between the partially ordered state and the completely disordered state in Fig. 5(b), weak streaks are observed at the positions of S1 spots in addition to main spots.

The formations of various types of approximant crystals have been reported for Al-Ni-Co (Ref. 22) and Al-

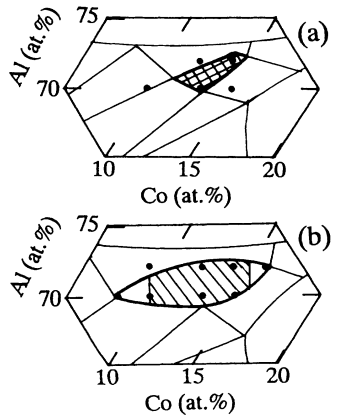

FIG. 5. Composition ranges of the three states of the decagonal phase at 650 °C (a) and at 850 °C (b): the completely ordered state (double-hatched area), the partially ordered state (single-hatched area) and the completely disordered state (open areas). Solid circles indicate the compositions of the samples studied.

Cu-Co (Ref. 23) alloys. Also in the present experiment, a trace of approximant crystals was detected by electron-diffraction experiments in the 850 °C-annealed samples with compositions at the Co-rich side in the single-decagonal-phase area. In principle, the single-approximant-phase areas should be added to the phase diagrams in Figs. 2(a) and 2(b). However, the exact location of them could not be determined from the present results. Further experiments are required to determine them.

Figures 6(a)–6(c) show electron-diffraction patterns with the incident beam along two kinds of twofold axes (P and D) perpendicular to the tenfold direction, taken from the 850 °C-annealed samples. The reciprocal basis vector along the tenfold direction $\mathbf{p}_5^*$ is indicated by an arrow in the D pattern in (a), showing a period of about 4.1 Å. The P pattern in (a) shows an extinction of the spots with h_5=odd (h_5 is the index referred to $\mathbf{p}_5^*$), which is attributable to a 10_5-screw symmetry accompanied by a c-glide symmetry. Most of the structure models proposed for Al-Ni-Co or Al-Cu-Co decagonal phases have a period of about 4 Å and a superspace group of $P10_5/mmc$,[24,25] which agrees with these patterns. In (b), weak streaks normal to the tenfold axis are seen at the positions corresponding to the double period (~8.2 Å) in both P and D patterns. In (c), the streaks appear to be more pronounced and considerably intense spots are observed at the positions with h_5=odd in the P pattern, indicating the disappearance of the 10_5-screw and the c-glide symmetries. Some of the structure models have a period of about 4 Å and a superspace group of $P10/mmm$,[26] which are consistent with the observed patterns in (c), except that weak spots are additionally observed at the positions with $h_5=n/2$ (n=odd) in the P pattern. The addition of the extra spots in Fig. 6(c) suggests that this structure corresponds to a superlattice structure with respect to the structure exhibiting the diffraction pattern in Figs. 6(a) or 6(b). Some atomic ordering between quasiperiodic planes is considered to be responsible for the formation of this type of superlattice structure. Similar variation of the twofold patterns has been reported for Al-Cu-Co alloys by Grushko, Wittmann, and Urban[27] As shown in Fig. 5, the three samples showing the patterns in Figs. 6 are in the completely disordered state for (a) and (c) and in the partially ordered state for (b). In addition, for the 650 °C-annealed $Al_{70}Ni_{17}Co_{13}$ sample, which is in the completely ordered state, we observed essentially the same type of P and D patterns as those in (b). These results indicate that the origin of the changes in the P and D patterns presented in Figs. 6 (a)–(c) is different from the origin of the in-quasiperiodic-plane order-disorder transformation shown in Figs. 3 (a)–(c).

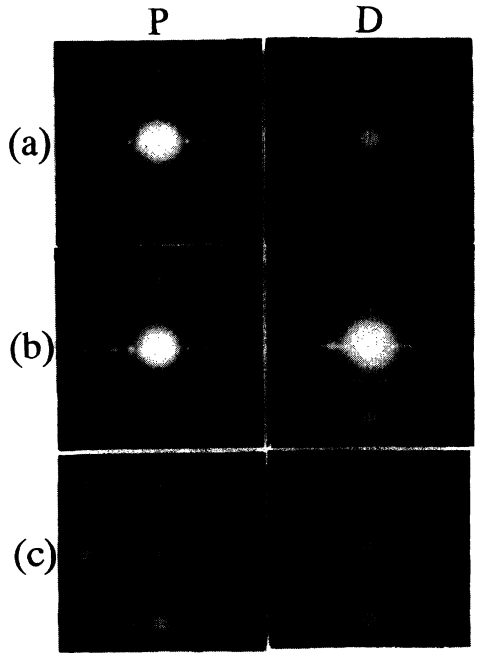

FIG. 6. Two kinds of twofold electron-diffraction patterns for 850 °C-annealed samples with the compositions of $Al_{70}Ni_{22}Co_8$ (a), $Al_{70}Ni_{17}Co_{13}$ (b), and $Al_{72}Ni_{11}Co_{16}$ (c). The tenfold axes are in the vertical direction in each pattern. The spot indicated by an arrowhead corresponds to the lattice spacing of about 2.1 Å. The reciprocal basis vector along the tenfold direction $\mathbf{p}_5^*$ is indicated by an arrow.

B. High-resolution electron microscopy

The high-resolution electron micrographs of decagonal phases have been shown to exhibit the arrangement of ringlike contrasts under a special condition: a slightly larger amount of defocus compared with the Scherzer defocus and relatively large sample thickness.[28] The ringlike contrast is considered to correspond to a columnar atomic cluster which itself has fivefold or tenfold symmetry. In this experiment, it is found that the ring contrast is markedly enhanced by reducing the size of aperture used for restricting diffraction spots contributing to imaging. Figures 7(a) and 7(b) show high-resolution electron micrographs taken from the same 850 °C-annealed $Al_{70}Ni_{22}Co_8$ sample. In Fig. 7(c), the sizes of the aperture used for the two micrographs are indicated on the electron-diffraction pattern taken from the same sample. The larger and smaller apertures correspond to the micrographs in Figs. 7(a) and 7(b), respectively. Comparing the micrographs of Figs. 7(a) and 7(b), we can see that reducing the size of the aperture remarkably enhances the ring contrast by suppressing the contrast of fine structures.

Figures 8(a) and 8(b) show high-resolution electron micrographs taken from the 650 °C-annealed $Al_{70}Ni_{17}Co_{13}$ and 850 °C-annealed $Al_{70}Ni_{22}Co_8$ samples, respectively. It is confirmed by the electron-diffraction experiment that the decagonal phases in Figs. 8(a) and 8(b) are in the ordered state and disordered one, respectively. The smaller aperture shown in Fig. 7(c) is used for these micrographs, with the result that the ring contrasts are clearly observed. We should note, however, that not all the ring contrasts have a perfect ring shape; some of them are separated into a few parts or others are considerably distorted. In Figs. 8(a) and 8(b), only the ring contrasts with comparably high perfection are selected and their centers

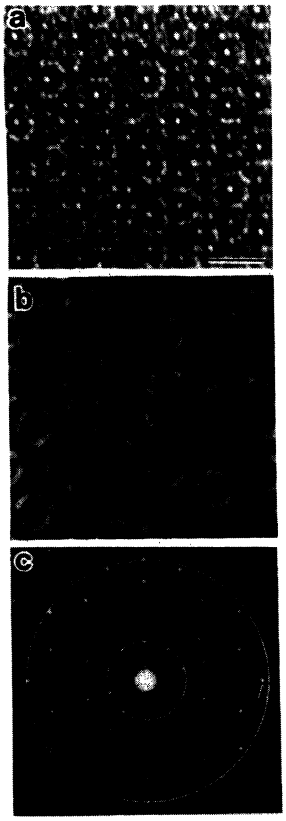

FIG. 7. High-resolution electron micrographs [(a) and (b)] and an electron-diffraction pattern (c) taken from the 850 °C-annealed $Al_{70}Ni_{22}Co_8$ sample. The incident beam is parallel to the tenfold axis. The marker in (a) corresponds to 20 Å. The arrowhead in (c) indicates the spot with the lattice spacing of about 2.0 Å. The sizes of the apertures used for the two micrographs in (a) and (b) are shown in (c); the larger and smaller apertures correspond to (a) and (b).

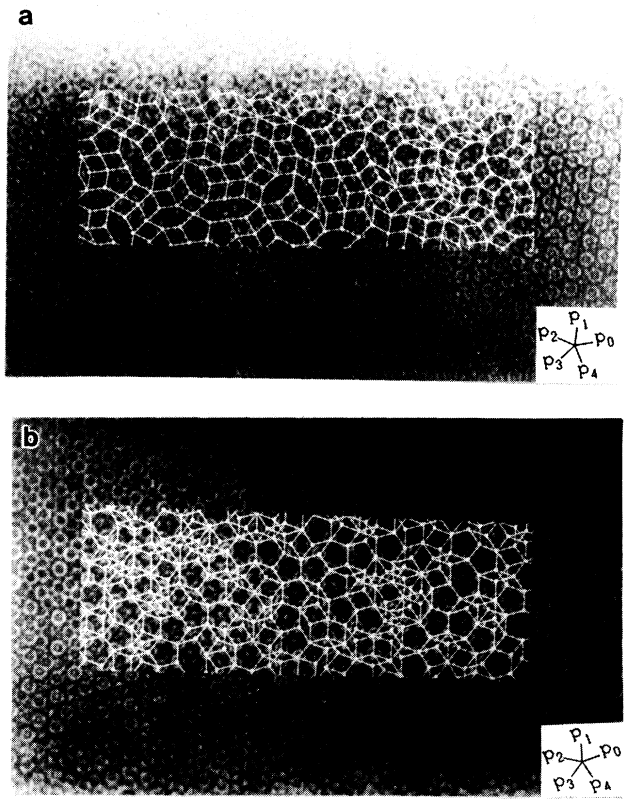

FIG. 8. High-resolution electron micrographs with the incident beam parallel to the tenfold axis, taken from the 650 °C-annealed $Al_{70}Ni_{17}Co_{13}$ (a) and 850 °C-annealed $Al_{70}Ni_{22}Co_8$ (b). The ring centers are connected by the five basis vectors $\mathbf{p}_i (i=0,\ldots,4)$ with the length of about 20 Å.

are connected by the five basis vectors $\mathbf{p}_i$ $(i=0,\ldots,4)$ with the length of about 20 Å. In addition, their arrangements extracted from larger portions including the regions of Figs. 8(a) and 8(b) are presented in Figs. 9(a) and 9(b), respectively. The tilting pattern in Fig. 9(a) consists mostly of three elements: two kinds of rhombus {fat and skinny rhombi in a rhombic Penrose tiling [Fig. 10(c)]} and a hexagon which can be divided into a fat rhombus and two skinny rhombi. This pattern contains very few numbers of regular pentagons. In the pattern in Fig. 9(b), we can see overlapping of the tiles at many places, reflecting the high density of the ring contrasts. In contrast to the pattern in Fig. 9(a), the pattern in Fig. 9(b) contains plenty of regular pentagons with two different sizes: a pentagon with the 20-Å edge and its $\tau[=(1+\sqrt{5})/2]$ times smaller pentagon forming a star shape in the figure. Similar HRTEM observation of the structure change in an Al-Ni-Co alloy has been reported by Hiraga, Lincoln, and Sun.[8] In their paper, the arrangements of the ring contrasts similar to those in Figs. 9(a) and 9(b) have been observed in 550 and 800 °C-annealed $Al_{70}Ni_{15}Co_{15}$ alloys, respectively. The slight difference in the density of the rings between our 850 °C-annealed sam-

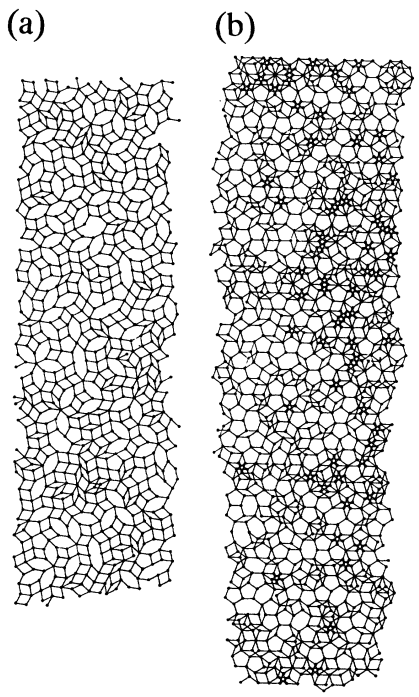

FIG. 9. The arrangements of the centers of ring contrasts for the 650 °C-annealed $Al_{70}Ni_{17}Co_{13}$ (a) and 850 °C-annealed $Al_{70}Ni_{22}Co_8$ (b).

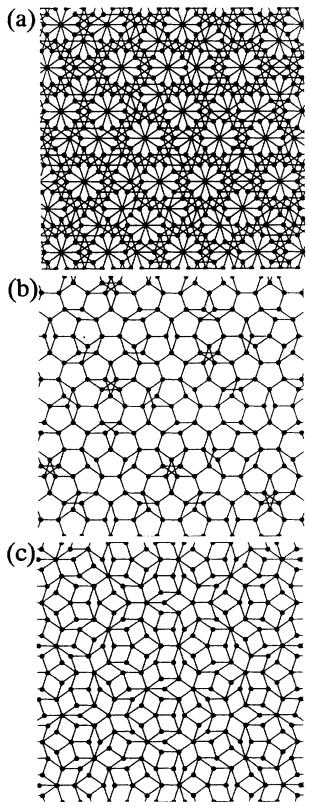

FIG. 10. Typical examples of the decagonal quasicrystalline tiling patterns: the Burkov tiling (a), the pentagonal Penrose tiling (b), and the rhombic Penrose tiling (c).

ple and their 800 °C-annealed sample is considered to be mainly due to the difference in the observation conditions, especially the size of the aperture described above. In our experiment, the density of the ring contrasts tends to become high due to the enhancement of the contrast.

In Figs. 10(a)–(c), typical examples of the decagonal quasicrystalline tiling pattern are presented. The pattern in Fig. 10(a) shows the arrangement of an atomic cluster in a structure model of the Al-Cu-Co and Al-Ni-Co decagonal quasicrystals proposed by Burkov.[24] We hereafter refer to this pattern as the Burkov tiling. Though Burkov's model is in principle a random tiling,[29] an "ideal" configuration is given in the cut-and-projection framework. In this model, decagonal atomic clusters with about 10-Å radius sit at the vertices of the Burkov tiling with the bond length of 20 Å. The patterns in Figs. 10(b) and 10(c) correspond to a pentagonal Penrose tiling and a rhombic Penrose tiling, respectively. Yamamoto has proposed another structure model, in which decagonal atomic clusters are arranged on the pentagonal Penrose tiling with the 20-Å bond.[25] Similarities should be pointed out between these typical tilings and the observed tilings in Figs. 9(a) and 9(b); the pattern in Fig. 9(a) is similar to the rhombic Penrose tiling and the pattern in Fig. 9(b) resembles the pentagonal Penrose tiling on the whole and also resembles the Burkov tiling partially.

In general, the vertices of the decagonal quasicrystalline tiling with the edge length of a can be expressed as $\mathbf{r}_{\parallel}=\sum_i n_i \mathbf{p}_i$, where n_i $(i=0,\ldots,4)$ are integers and $\mathbf{p}_i=a[\cos(2i\pi/5),\sin(2i\pi/5)]$ $(i=0,\ldots,4)$. To ensure the one-to-one correspondence between $\mathbf{r}_{\parallel}$ and (n_0,n_1,n_2,n_3,n_4), we should impose the condition that (n_0,n_1,n_2,n_3,n_4) satisfy $\sum_i n_i=0,\pm1$ or ±2. The procedure of determining five-dimensional lattice points (n_0,n_1,n_2,n_3,n_4) from the set of points $\mathbf{r}_{\parallel}$ using the above relations is called "lifting." Projection of the lifted (n_0,n_1,n_2,n_3,n_4) onto the "perp-space" is performed by calculating $\mathbf{r}_{\perp}=\sum_i n_i \mathbf{q}_i$, where $\mathbf{q}_i$ are defined as $\mathbf{q}_i=\mathbf{p}_{(2i \bmod 5)}$ $(i=0,\ldots,4)$.[30] For the ideal decagonal quasicrystalline tilings with the point-group symmetry $10mm$, the following conditions should be satisfied:[12,17] (1) The five sets of points $A_m=\{\mathbf{r}_{\perp}=\sum_i n_i \mathbf{q}_i \mid \sum_i n_i=m\}$ $(m=0,\pm1$ and $\pm2)$ are distributed densely within five bounded domains α_m $(m=0,\pm1$ and $\pm2)$, respectively. (2) α_0 has the point-group symmetry of $10mm$ and the other four domains have $5m$ symmetry, each pair of domains $\alpha_{\pm1}$ and $\alpha_{\pm2}$ being related by the inversion operation.[31]

In Figs. 11(a) and 11(b), the five sets of points $A_m=\{\mathbf{r}_{\perp}=\sum_i n_i \mathbf{q}_i \mid \sum_i n_i=m\}$ $(m=0,\pm1$ and $\pm2)$ deduced from the tilings in Figs. 9(a) and 9(b) are presented and in Fig. 11(c) the domains α_m $(m=0,\pm1$ and $\pm2)$ for the patterns in Figs. 10(a)–10(c) are shown for comparison. The Burkov tiling and the pentagonal Penrose tiling have regular decagons with the same sizes for all the domains. The sizes for the two tilings differ by a factor of 1.38. In contrast, the rhombic Penrose tiling has different domains: none for α_0, oppositely directed regular pentagons for $\alpha_{\pm1}$, and their τ-times larger pentagons for $\alpha_{\pm2}$.[12,17] It should be noted that the domains for all the three tilings satisfy the condition (2) described above. Between the point distributions in Fig. 11(a) and those in Fig. 11 (b), we notice striking contrasts:

(1) The numbers of points and the spatial extensions of the point distributions for the five sets differ remarkably in (a), whereas they are approximately the same in (b).

(2) The spatial extensions of the point distributions in (a) are much wider compared with those in (b).

The latter result in (1) is related to the fact that the tiling pattern in Fig. 9(b) has plenty of regular pentagons; each vertex of a regular pentagon contributions to each of the five domains separately. In contrast, an abundance of rhombi in the pattern in Fig. 9 (a) leads to the former result in (1). As discussed by Ishihara and Yamamoto,[17] the rhombic Penrose tiling, which has five different domains, can be regarded as a superlattice structure with respect to the structures in which all the domains have the same size and shape, as in the Burkov tiling and the pentagonal Penrose tiling. In fact, the reciprocal lattice of the rhombic Penrose tiling with the 20-Å edge coincides with that spanned by $\mathbf{p}_i^{*\prime}$ in Fig. 4, while the reciprocal lattices of the other two patterns with the same edge length coincide with that spanned by $\mathbf{p}_i^{*}$.[32] Though somewhat scattered point distributions in Figs. 11(a) and 11(b) do not allow us to determine the exact shapes of the domains α_m $(m=0,\ \pm1,$ and $\pm2)$, the result (1) clearly

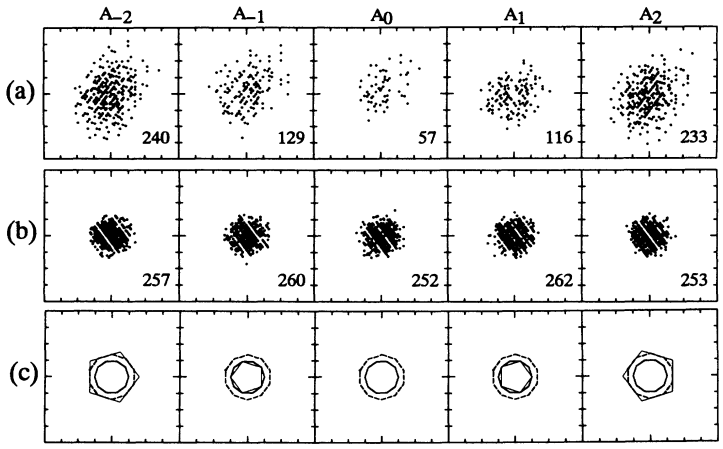

FIG. 11. (a) and (b): projection of the lifted points onto the perp-space for the tilings in Figs. 9(a) and 9(b); (c): the domains for the tiling patterns in Figs. 10(a)–(c). The unit in the axes corresponds to $|\mathbf{q}_i^*|$. The number of points is shown in each domain in (a) and (b). In (c), the domains for the Burkov tiling, the pentagonal Penrose tiling, and the rhombic Penrose tiling are shown by broken thick lines, simple thick lines, and simple thin lines, respectively.

indicates that the change in the tiling structure of the atomic cluster is responsible for the present case of order-disorder structural transformation.

The result (2) indicates that the tiling in Fig. 9(a), which is observed in the 650 °C-annealed sample, contains a larger amount of phason strain than that in Fig. 9(b) observed in the 850 °C-annealed sample. Such a large amount of phason strain in the pattern in Fig. 9(a) is evidenced also by the appearance of clusterings of several rhombic tiles of the same type. A similar temperature dependence of the amount of phason strain has been reported for Al-Ni-Co alloys by Hiraga, Lincoln, and Sun and for Al-Cu-Co alloys by Hiraga, Sun, and Lincoln[33] and by Chen *et al.*[34] They have discussed the results in light of a random tiling model,[29] which predicts that the phason fluctuation in quasicrystals grows with decreasing temperature. However, it is still unclear how the present case of the decagonal quasicrystal, which has two-dimensional quasiperiodicity plus one-dimensional periodicity, should be treated in terms of the random tiling model. In particular, we should note the following facts in comparing the phason disorders in the patterns of Figs. 9(a) and 9(b): (1) the alloy compositions are considerably different, and (2) the phason disorder may not reach thermal equilibrium in the 650 °C-annealed sample.

In general, the superlattice order in a quasicrystal is introduced by differentiating the domains for different sublattices of the high-dimensional periodic lattice, as described above. The domains have a two-dimensional shape for two-dimensional quasicrystals and contain information on positions of infinite numbers of atoms (or atomic clusters). This is in contrast to the case of conventional crystals, in which decoration of each lattice point is made with a limited number of atoms. The differentiation of the domains can induce a global rearrangement of the atoms (or atomic clusters), as shown in Figs. 9(a) and 9(b), which is a new type of superlattice ordering characteristic of the quasicrystal.

IV. CONCLUSIONS

The formation ranges of the Al-Ni-Co decagonal quasicrystals with and without the in-quasiperiodic-plane superlattice order have been investigated. The single-decagonal-phase region at 650 °C is limited to a very small area around $Al_{71}Ni_{16}Co_{13}$, which expands almost along an Al-constant line at 850 °C. The single-decagonal-phase area at 650 °C entirely yields the completely ordered state, while that at 850 °C yields either a partially ordered state or the completely disordered state. Besides the in-quasiperiodic-plane ordering, an atomic ordering between quasiperiodic planes was found. The degree of the latter ordering increases monotonically with decreasing Co content, which is not relevant to the compositional dependence of the former ordering. This fact indicates that the two kinds of ordering have different origins.

The decagonal quasicrystalline structures with and without the in-quasiperiodic-plane superlattice order have been observed by high-resolution transmission electron microscopy. Both images comprise the arrangements of ringlike contrasts, forming tiling patterns with a 20-Å edge. These tiling patterns have been analyzed on the basis of a high-dimensional description of the quasicrystalline structure. The projection of the vertices of the tiles onto the perp-space exhibits striking contrasts between the two structures; the structure with the superlattice order gives nonequivalent distributions for the five different sites, while the structure without the order gives approximately the same distributions for them. This results leads to the conclusion that the rearrangement of the atomic cluster giving the ring contrast in the HRTEM image is responsible for the order-disorder structural transformation in the Al-Ni-Co decagonal quasicrystals. This type of structural transformation is a new type of order-disorder transformation characteristic of quasicrystals.

ACKNOWLEDGMENTS

The authors would like to thank H. Nishioka and K. Ibe of JEOL and M. Ichihara of ISSP, the University of Tokyo for their cooperation in the electron-diffraction experiments. This work has been supported by a Grant-in-Aid for Scientific Research from the Ministry of Education, Science, and Culture.

[1]L. Bendersky, Phys. Rev. Lett. **55**, 1461 (1985); K. Chattopadhyay, S. Ranganathan, G. N. Subbanna, and N. Thangaraj, Scr. Metall. **19**, 767 (1985).

[2]L. X. He, Y. K. Wu, and K. H. Kuo, J. Mater. Sci. Lett. **7**, 1284 (1987); A. P. Tsai, A. Inoue, and T. Masumoto, Mater. Trans. JIM **30**, 463 (1989).

[3]A. Inoue, A. P. Tsai, and T. Masumoto, in *Quasicrystals,* edited by T. Fujiwara and T. Ogawa, Springer Series in Solid State Science Vol. 93 (Springer-Verlag, Berlin, 1990), p. 80.

[4]C. Beeli, H.-U. Nissen, and J. Robadey, Philos. Mag. Lett. **63**, 87 (1991).

[5]A. P. Tsai, A. Inoue, and T. Masumoto, Philos. Mag. Lett. **64**, 163 (1991).

[6]For a recent review, see W. Steurer, Mater. Sci. Forum **150-151**, 15 (1994).

[7]C. L. Henley, J. Non-Cryst. Solids **153-154**, 172 (1993). (This presents many structure models, which are originally described in diverse ways by different authors, in a unified picture.)

[8]K. Hiraga, F. J. Lincoln, and W. Sun, Mater. Trans. JIM **32**, 308 (1991).

[9]K. Hiraga and W. Sun, Philos. Mag. Lett. **67**, 117 (1993).

[10]R. S. Becker and A. Kortan, in *Quasicrystals: The State of the Art,* edited by D. P. DiVincenzo and P. J. Steinhardt (World Scientific, Singapore, 1991), p. 111.

[11]P. Bak, Phys. Rev. Lett. **56**, 861 (1986).

[12]T. Janssen, Acta Crystallogr. A **42**, 261 (1986).

[13]K. Edagawa, M. Ichihara, K. Suzuki, and S. Takeuchi, Philos. Mag. Lett. **66**, 19 (1992).

[14]K. Edagawa, H. Sawa, M. Ichihara, K. Suzuki, and S. Takeuchi, Mater. Sci. Forum **150-151**, 223 (1994).

[15]K. Edagawa, H. Sawa, and S. Takeuchi, Philos. Mag. Lett. **69**, 227 (1994).

[16]K. Edagawa, K. Suzuki, M. Ichihara, and S. Takeuchi, Microsc. Microanal. Microstruct. **4**, 341 (1993).

[17]K. N. Ishihara and A. Yamamoto, Acta Crystallogr. A **44**, 508 (1988).

[18]K. Niizeki, J. Phys. A **22**, 4281 (1989); **23**, 4569 (1990).

[19]F. Lancon, L. Billard, S. E. Burkov, and M. de Boissien, J. Phys. I (France) **4**, 283 (1994).

[20]A. J. Bradley and A. Taylor, Philos. Mag. **23**, 1049 (1937).

[21]T. C. Lubensky, J. E. S. Socolar, P. J. Steinhardt, P. A. Bancel, and P. A. Heiney, Phys. Rev. Lett. **57**, 1440 (1986).

[22]K. Edagawa, M. Ichihara, K. Suzuki, and S. Takeuchi, J. Non-Cryst. Solids **153-154**, 19 (1993).

[23]T. L. Daulton and K. F. Kelton, Philos. Mag. Lett. **63**, 257 (1991); C. Dong, J. M. Dubois, S. S. Kang, and M. Audier, Philos. Mag. B **65**, 107 (1992).

[24]S. E. Burkov, Phys. Rev. Lett. **67**, 614 (1991).

[25]A. Yamamoto (unpublished).

[26]A. Yamamoto, K. Kato, T. Shibuya, and S. Takeuchi, Phys. Rev. Lett. **65**, 1603 (1990).

[27]B. Grushko, R. Wittmann, and K. Urban, Philos. Mag. Lett. **67**, 25 (1993).

[28]K. Hiraga, in *Quasicrystals: The State of the Art* (Ref. 10), p. 95.

[29]For a review, see C. L. Henley, in *Quasicrystals: The State of the Art* (Ref. 10), p. 429.

[30]Y. He, H. Chen, S. J. Poon, and G. Shiflet, Philos. Mag. Lett. **64**, 307 (1991).

[31]α_m ($m=0,\pm1$, and ±2) are interchanged cyclically depending on the selection of the origin. However, we are always able to find an appropriate origin so that the tiling with $10mm$ symmetry satisfies the condition (2).

[32]This can be proven by taking into account the fact that $\tau^n \mathbf{p}_i^*$ ($i=1,\ldots,4$) for every integer n span exactly the same reciprocal lattice.

[33]K. Hiraga, W. Sun, and F. J. Lincoln, Jpn. J. Appl. Phys. **30**, L302 (1991).

[34]H. Chen, S. E. Burkov, Y. He, S. J. Poon, and G. J. Shiflet, Phys. Rev. Lett. **65**, 72 (1990).

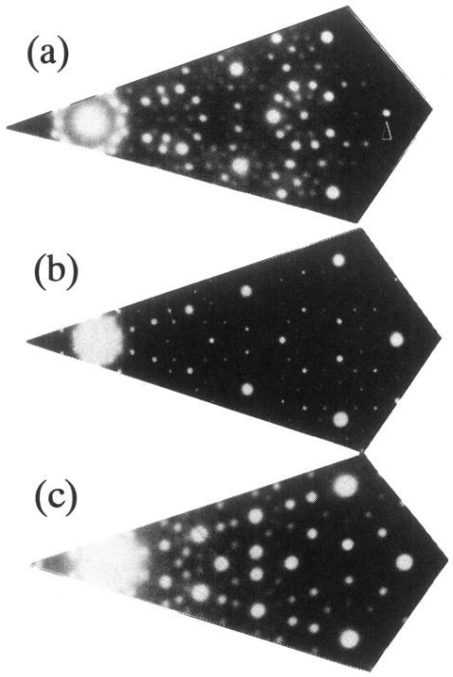

FIG. 3. $\frac{1}{10}$ sections of the tenfold electron-diffraction patterns for the 650 °C-annealed $Al_{70}Ni_{17}Co_{13}$ (a), 850 °C-annealed $Al_{70}Ni_{17}Co_{13}$, (b) and 850 °C-annealed $Al_{70}Ni_{22}Co_8$ (c) samples. The spot corresponding to the lattice spacing of about 2.0 Å is indicated by an arrowhead.

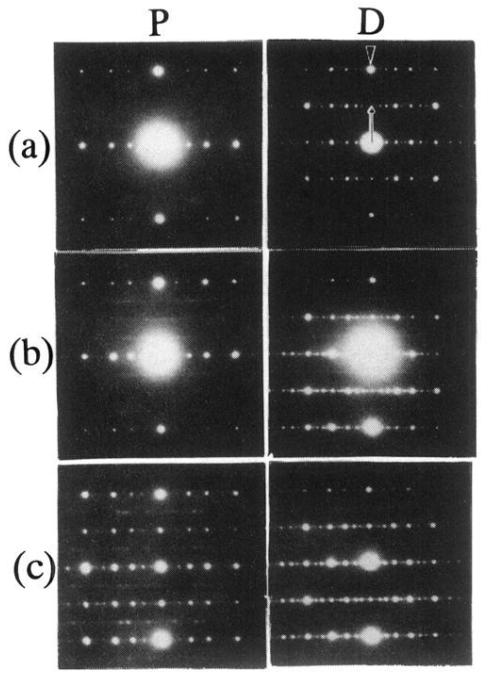

FIG. 6. Two kinds of twofold electron-diffraction patterns for 850°C-annealed samples with the compositions of $Al_{70}Ni_{22}Co_8$ (a), $Al_{70}Ni_{17}Co_{13}$ (b), and $Al_{72}Ni_{11}Co_{16}$ (c). The tenfold axes are in the vertical direction in each pattern. The spot indicated by an arrowhead corresponds to the lattice spacing of about 2.1 Å. The reciprocal basis vector along the tenfold direction $\mathbf{p}_5^*$ is indicated by an arrow.

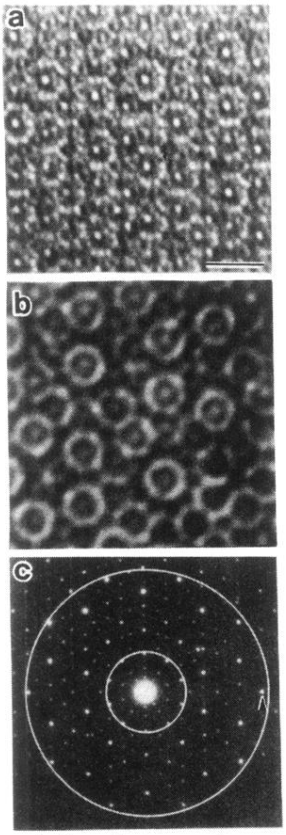

FIG. 7. High-resolution electron micrographs [(a) and (b)] and an electron-diffraction pattern (c) taken from the 850 °C-annealed $Al_{70}Ni_{22}Co_8$ sample. The incident beam is parallel to the tenfold axis. The marker in (a) corresponds to 20 Å. The arrowhead in (c) indicates the spot with the lattice spacing of about 2.0 Å. The sizes of the apertures used for the two micrographs in (a) and (b) are shown in (c); the larger and smaller apertures correspond to (a) and (b).

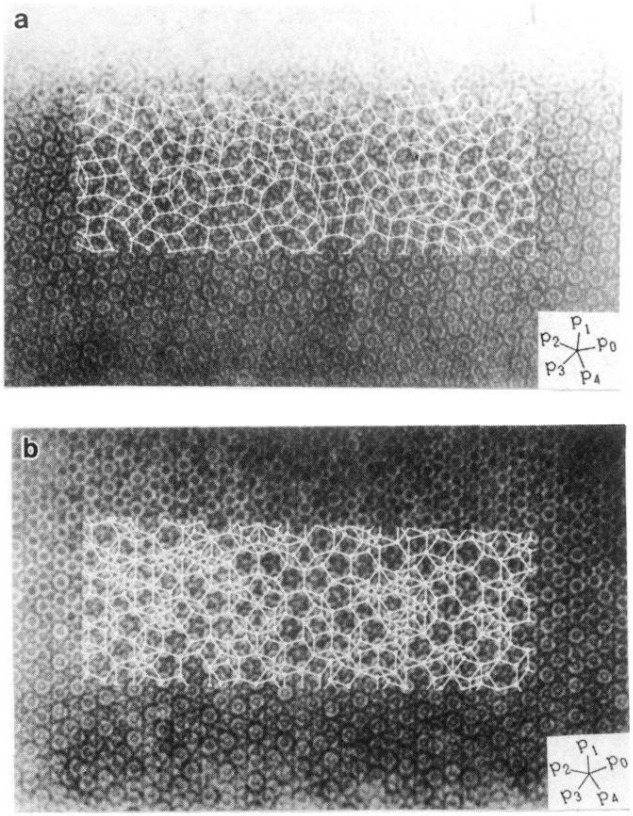

FIG. 8. High-resolution electron micrographs with the incident beam parallel to the tenfold axis, taken from the 650 °C-annealed $Al_{70}Ni_{17}Co_{13}$ (a) and 850 °C-annealed $Al_{70}Ni_{22}Co_8$ (b). The ring centers are connected by the five basis vectors $\mathbf{p}_i (i = 0, \ldots, 4)$ with the length of about 20 Å.